New Journal of Physics
The open-access journal for physics

Ultrafast nanoplasmonics under coherent control

Mark I Stockman

Department of Physics and Astronomy, Georgia State University, Atlanta, GA 30303, USA
E-mail: mstockman@gsu.edu

New Journal of Physics **10** (2008) 025031 (20pp)
Received 9 November 2007
Published 29 February 2008
Online at http://www.njp.org/
doi:10.1088/1367-2630/10/2/025031

Abstract. Recently, there has been an increased attention and rapid development in the field of nanoscale collective electronic dynamics on surfaces of metal nanostructures, which is due to excitations called surface plasmons (SPs). This field, known as nanoplasmonics, is very promising for such applications as the next generation optoelectronics, computations and information storage on the nanoscale, ultrasensitive detection of threats and spectroscopy of physical, chemical and biological nano-objects. Due to their broad spectral bandwidth, SPs possess ultrafast dynamics, with times as short as hundreds of attoseconds. In this paper, we discuss progress in the excitation, control and applications of the ultrafast nanoplasmonic fields. Special attention is devoted to attosecond visualization and coherent control of the nanoscale optical fields. Prospective applications of ultrafast nanoplasmonics are discussed.

Contents

1. Introduction

Nanooptics and nanoplasmonics are experiencing presently a period of explosive growth and attract a great interest. Nanoplasmonics deals with electronic processes at the surfaces of metal nanostructures, which are due to electronic excitations called surface plasmons (SPs) that can localize optical energy on the nanoscale [1]–[3]. The nanoplasmonic processes can potentially be the fastest in optics: their shortest evolution times are defined by the inverse spectral width $\Delta\omega^{-1}$ of the region of the plasmonic resonances ($\Delta\omega \approx 4\,\mathrm{eV}$) and are on the order of hundreds of attoseconds [4]. The dephasing times of the SP excitations are also ultrashort, in the 10–100 fs range [5]–[9]. Such nanolocalization and ultrafast kinetics make plasmonic nanostructures promising for various applications, especially for ultrafast computations, data control and storage on the nanoscale.

These and many other applications require precise control over the optical excitations of the nanostructures in time and space on the femtosecond–nanometre scale. Such a control at optical frequencies is difficult to impose with conventional metal nanowires leads. The bandwidth of the nanowire transmission may not be sufficient, the dispersion and delay are significant, and losses of nanowaveguides are large. An even more serious problem is posed by cross-talk: the capacitive coupling between different nanowires connected to a nanosystem is large, proportionally to frequency, at optical frequencies. One of the possibilities to connect a nanosystem to far-field sources of energy is to use tapered adiabatic waveguides [10]–[13]. Another approach is using the so-called hyperlenses, which are anisotropic media consisting of layers of metal and dielectrics that connect the far-field radiation and near-field (local field) zone [14]. All these methods invoke external metal objects in the nano-vicinity of the

nanosystem, which may be perturbing: they would induce non-radiative and radiative losses and cross-talk between parts of the nanosystem.

Therefore, it would be desirable to control the plasmonic nanostructures with light wirelessly, with far-field electromagnetic radiation. However, such radiation cannot be focused on the nanoscale. In other words, the optical radiation does not have spatial degrees of freedom on the nanoscale. However, it has phase, amplitude and polarization degrees of freedom. The idea to control the spatial distribution of the optical energy on the nanoscale by the phase modulation of the incident wave has been proposed [15, 16]. The phase, polarization and amplitude modulation proved to be efficient degrees of freedom in controlling the local fields [15]–[21].

In this paper, we review from unified positions the latest theoretical ideas and developments in the field of coherent control on the nanoscale. The paper is organized as follows. In section 2, we discuss both qualitative ideas and summarize the main points of the quantitative theory. In section 3, we discuss the recently proposed idea of the attosecond nanoplasmonic field microscope [4]. The presentation is made more self-contained by the related details of the theory presented in section 2; also, this approach is contrasted to recently published materials on hyperlenses. In section 4, we present a new approach to ultrafast coherent control on the nanoscale based on the idea of the time reversal [22].

2. Theory of the coherent control on the nanoscale

2.1. Qualitative physics

The physics of the coherent control of the nanoscale energy localization can be described as directed interference of the SPs excited by the incident plane wave $\mathbf{E}_0(t)$, which does not have any spatial dependence on the scale of the nanosystem. This excitation waveform by its phase and amplitude at different frequencies ω, i.e. by its amplitude in the Fourier space $\mathbf{E}_0(\omega)$, imparts the phase and amplitude on the correspondingly localized SPs eigenmodes. These SPs interfere in real space (on the nanoscale) and time (on intervals of a fraction of the inverse bandwidth $\Delta\omega^{-1}$, i.e. hundreds of attoseconds). This interference depends on the phases and amplitudes of the SPs oscillations and is therefore coherently controllable by the excitation waveform $\mathbf{E}_0(t)$.

It is easy to estimate the maximum number of the degrees of freedom contained in a modulated optical pulse. The time of the phase memory of the system is defined by the dephasing time, which is an inverse relaxation rate of the optical (dipole) polarization γ. This polarization relaxation rate for SPs has been found in [23] as

$$\gamma(\omega) = \frac{\operatorname{Im}\varepsilon_{\mathrm{m}}(\omega)}{\operatorname{Re}\left(\partial\varepsilon_{\mathrm{m}}(\omega)/\partial\omega\right)}, \tag{1}$$

where $\varepsilon_m(\omega)$ is the frequency-dependent dielectric permittivity of the plasmonic metal. Each half-period of the excitation field oscillations within the interval of $\gamma(\omega)^{-1}$ defines two characteristic variables: the instantaneous amplitude and the instantaneous period for each of the two polarizations, overall four degrees of freedom. Thus the maximum number of the degrees of freedom is

$$N_{\mathrm{df}} = \frac{4}{\pi}\frac{\omega}{\gamma} \sim Q = \omega\frac{\operatorname{Re}\left(\partial\varepsilon_{\mathrm{m}}(\omega)/\partial\omega\right)}{\operatorname{Im}\varepsilon_{\mathrm{m}}(\omega)}, \tag{2}$$

where $Q = \omega/\gamma(\omega)$ is the quality factor of the plasmonic oscillations. For example, for the best plasmonic metal, silver, this factor is of the order of several tens for the most of the visible

region. This provides a significant number of the degrees of freedom to control the nanoscale distribution of the local fields in space and time.

2.2. Spectral Green's function theory of coherent control on the nanoscale

Below in this section, for the sake of completeness and convenience, we outline obtaining Green's function theory of the coherent control on the nanoscale. We base our consideration on the framework of spectral theory [3, 16, 24]. Consider a system consisting of a metal with dielectric permittivity $\varepsilon(\omega)$ embedded in a dielectric background with dielectric constant ε_{d}. The geometry of the system is described by the characteristic function $\Theta(\mathbf{r})$, which equals 1 in the metal and 0 in the dielectric.

For a nanosystem, which has all sizes much less than the relevant electrodynamic dimensions (radiation wavelength across the propagation direction of the excitation wave and the skin depth in this direction), the quasistatic approximation is applicable. In such a case, we can take into account only the static optical potential $\varphi(\mathbf{r}, t)$. In the frequency domain, it satisfies the continuity equation

$$\left[\frac{\partial}{\partial \mathbf{r}}\Theta(\mathbf{r})\frac{\partial}{\partial \mathbf{r}} - s(\omega)\frac{\partial^2}{\partial \mathbf{r}^2}\right]\varphi(\mathbf{r}, \omega) = 0, \tag{3}$$

where $s(\omega) = (1 - \varepsilon_{\mathrm{m}}(\omega)/\varepsilon_{\mathrm{d}})^{-1}$ is the spectral parameter [25].

At the boundary of the system, we impose boundary conditions. There may be two types of them; firstly the Dirichlet conditions,

$$\varphi(\mathbf{r}, \omega) = \varphi_0(\mathbf{r}, \omega), \quad \text{for } \mathbf{r} \in \Gamma, \tag{4}$$

where Γ denotes the boundary, and $\varphi_0(\mathbf{r}, \omega)$ is the external (excitation) electric field potential. The second type are the mixed Dirichlet–Neumann boundary conditions,

$$\begin{aligned} &\varphi(\mathbf{r}, \omega) = \varphi_0(\mathbf{r}, \omega), \quad \text{for } \mathbf{r} \in \Gamma_{\perp}, \\ &\frac{\partial \varphi(\mathbf{r}, \omega)}{\partial \mathbf{r_n}} = 0, \quad \text{for } \mathbf{r} \in \Gamma_{\parallel}, \end{aligned} \tag{5}$$

where $\Gamma_{\perp}$ denotes the planes of the boundary that are normal to the external field, and $\Gamma_{\parallel}$ denotes those parallel to the external field; $\mathbf{r_n}$ is the vector normal to the surface.

Green's function satisfies a similar equation with the δ-function on the right-hand side

$$\left[\frac{\partial}{\partial \mathbf{r}}\Theta(\mathbf{r})\frac{\partial}{\partial \mathbf{r}} - s(\omega)\frac{\partial^2}{\partial \mathbf{r}^2}\right]\bar{G}^{\mathrm{r}}(\mathbf{r}, \mathbf{r}'\omega) = \delta(\mathbf{r} - \mathbf{r}') \tag{6}$$

and homogeneous Dirichlet or Dirichlet–Neumann boundary conditions, i.e. equation (4) or (5) with the zero right-hand side parts.

It is convenient to expand the Green's function over eigenmodes $\varphi_n(\mathbf{r})$ and the corresponding eigenvalues s_n that satisfy a homogeneous counterpart of equation (3)

$$\left[\frac{\partial}{\partial \mathbf{r}}\Theta(\mathbf{r})\frac{\partial}{\partial \mathbf{r}} - s_n\frac{\partial^2}{\partial \mathbf{r}^2}\right]\varphi_n(\mathbf{r}) = 0, \tag{7}$$

with the homogeneous boundary conditions. This spectral expansion of the Green's function can be readily obtained from equation (6). It has an explicit form

$$\bar{G}^{\mathrm{r}}(\mathbf{r}, \mathbf{r}'; \omega) = \sum_n \frac{\varphi_n(\mathbf{r})\, \varphi_n(\mathbf{r}')^*}{s(\omega) - s_n}. \tag{8}$$

Two features of this expansion are important. First, it separates the dependencies on geometry and material properties. The geometrical properties of the nanosystem enter only through the eigenfunctions φ_n and eigenvalues s_n that are independent of the material properties of the system. Therefore, they can be computed for a given geometry once and stored, which simplifies and accelerates further computations. Complementarily, the material properties of the system enter equation (8) only through a single function: spectral parameter s_n.

The second important feature is that this Green's function satisfies exact analytical properties due to the form of equation (8) that contains only simple poles in the lower half-plane of the complex frequency ω and does not have any singularities in the upper half-plane of ω. Consequently, $\bar{G}^{\mathrm{r}}$ is a retarded Green's function that automatically guarantees the causality of the results of time-dependent calculations. Namely, $\bar{G}^{\mathrm{r}}(\mathbf{r}, \mathbf{r}'; t) = 0$ for $t < 0$.

Having this Green's function, we can find the local field potential $\varphi(\mathbf{r}, \omega)$ generated by the nanosystem in response to any excitation field (external potential) $\varphi_0(\mathbf{r}, \omega)$,

$$\varphi(\mathbf{r}) = \varphi_0(\mathbf{r}, \omega) - \int_V \varphi_0(\mathbf{r}', \omega) \frac{\partial}{\partial \mathbf{r}'} \Theta(\mathbf{r}') \frac{\partial}{\partial \mathbf{r}'} \bar{G}^{\mathrm{r}}(\mathbf{r}, \mathbf{r}'; \omega)\, \mathrm{d}^3 r'. \tag{9}$$

We can also introduce the retarded tensor Green's function $G^{\mathrm{r}}_{\alpha\beta}$ in terms of the corresponding scalar Green's function $\bar{G}^{\mathrm{r}}$:

$$G^{\mathrm{r}}_{\alpha\beta}(\mathbf{r}, \mathbf{r}'; \omega) = \frac{\partial^2}{\partial r_\alpha \partial r'_\beta} \bar{G}^{\mathrm{r}}(\mathbf{r}, \mathbf{r}'; \omega), \tag{10}$$

where $\alpha, \beta = x, y, z$, are vector indices. This tensor determines components of the dyadic Green's function $\mathbf{G}$ as $(\mathbf{G}^{\mathrm{r}})_{\alpha\beta} = G^{\mathrm{r}}_{\alpha\beta}(\mathbf{r}, \mathbf{r}'; \omega)$.

For excitation from a far zone, the external field $\mathbf{E}_0$ in the vicinity of the nanosystem is uniform, $\varphi_0(\mathbf{r}, \omega) = -\mathbf{E}_0(\omega)\mathbf{r}$. Taking this into account and Fourier transforming equation (9) to the time domain, we obtain the resulting local optical electric field $\mathbf{E}$ at the nanosystem in terms of the dyadic Green's function $\mathbf{G}^{\mathrm{r}}$ as

$$\mathbf{E}(\mathbf{r}, t) = \mathbf{E}_0(\mathbf{r}, t) + \int \mathrm{d}^3 r' \mathrm{d}t' \mathbf{G}^{\mathrm{r}}(\mathbf{r}, \mathbf{r}'; t - t') \Theta(\mathbf{r}') \mathbf{E}_0(t'), \tag{11}$$

where the integration over coordinates $\mathbf{r}'$ is extended over the entire volume of the system, and the integration over time t' is running over the duration of the excitation pulse.

We will also need the reaction of the system to a source of dielectric polarization $\mathbf{P}(\mathbf{r}, t)$. To find it, we consider the continuity equation (3) where the right-hand side is changed to $4\pi(\partial \mathbf{P}/\partial \mathbf{r})/\varepsilon_{\mathrm{d}}$. Applying the Green's function to this equation, we obtain the resulting local potential as

$$\varphi^{\mathrm{L}}(\mathbf{r}, \omega) = \frac{4\pi}{\varepsilon_{\mathrm{d}}} \int \mathrm{d}^3 r' G^{\mathrm{r}}(\mathbf{r}, \mathbf{r}'; \omega) \frac{\partial \mathbf{P}(\mathbf{r}', \omega)}{\partial \mathbf{r}'}. \tag{12}$$

Employing the Gauss theorem (integrating by parts), we find the corresponding local field,

$$\mathbf{E}^{\mathrm{L}}(\mathbf{r},\omega)=\frac{4\pi}{\varepsilon_{\mathrm{d}}}\int \mathrm{d}^3r'\mathbf{G}^{\mathrm{r}}(\mathbf{r},\mathbf{r}';\omega)\mathbf{P}(\mathbf{r}',\omega), \tag{13}$$

where we use the dyadic notations. For an oscillating point dipole $\mathbf{d}(t)$ at a position $\mathbf{r}_0$, we have $\mathbf{P}(\mathbf{r},t)=\delta(\mathbf{r}-\mathbf{r}_0)\mathbf{d}(t)$. Using this to eliminate the integration in equation (13) and transforming it to the time domain, we obtain

$$\mathbf{E}^{\mathrm{L}}(\mathbf{r},t)=\frac{4\pi}{\varepsilon_{\mathrm{d}}}\int \mathrm{d}t'\mathbf{G}^{\mathrm{r}}(\mathbf{r},\mathbf{r}_0;t-t')\,\mathbf{d}(\mathbf{r}_0,t'). \tag{14}$$

3. Attosecond nanoplasmonic field microscope [4]

3.1. Introduction of principles

Recently significant attention has been devoted to the development of attosecond science and technology, namely pulse generation, physical system excitation, detection, spectroscopy and electron motion control on the attosecond timescale [26]–[38].

The proposed attosecond nanoplasmonic field microscope [4] combines two modern techniques: photoelectron emission microscopy (PEEM) and attosecond streaking spectroscopy [39]. A plasmonic nanostructure is excited by an intense, waveform-controlled field in the optical spectral range that drives collective electron oscillations (SPs). This generates optical fields localized on the nanometre scale. An attosecond extreme ultraviolet (XUV) pulse, which is produced from and synchronized with the driving optical pulse, is then sent to the system.

This XUV pulse produces photoelectrons that, owing to their large energy and short emission time (determined by the attosecond pulse duration), escape from the nanometre-sized regions of local electric fields enhanced by plasmon resonances within a fraction of the oscillation period of the driven plasmonic field. The ultrashort escape time implies a final energy change of the emitted photoelectrons that is proportional to the local electric potential at the surface at the instant of electron release. This is in sharp contrast to previous attosecond streaking experiments performed in macroscopic volumes of gas-phase media, where the electron escape times are longer than the optical period; consequently, the change in electron energy probes the vector potential of the optical field [39]. For nanoplasmonic systems, the imaging of the emitted XUV-induced photoelectrons by an energy-resolving photoelectron emission microscope probes the electric field at the surface as a function of the XUV pulse incidence time and the position at the surface with an attosecond temporal and nanometre-scale spatial resolution.

3.2. Electron acceleration by nanoplasmonic fields

Let us discuss different regimes of the electron emission by an XUV pulse to identify those realistic for our conditions and conducive to our goals. The escape velocity for an electron can be estimated as $v_{\mathrm{e}}=\sqrt{2(\hbar\omega_{\mathrm{XUV}}-W_{\mathrm{f}})/m}$, where m is the electron mass, ω_{XUV} is the frequency of the XUV pulse, and W_{f} is the metal workfunction. The electron escape time from a region of local field of size b is $\tau_{\mathrm{e}}=b/v_{\mathrm{e}}$. The most important case for our purposes is the one to

be called a regime of instantaneous acceleration, when an electron leaves the local field region much faster than this field oscillates in time, i.e.

$$\tau_e \ll T, \tag{15}$$

where $T = 2\pi/\omega$ is a characteristic period of the optical excitation, and ω is the excitation pulse carrier frequency.

Under this condition, an electron is driven by a nearly frozen, instantaneous local electrostatic potential $\varphi(\mathbf{r}, t_{XUV})$, where t_{XUV} is the emission time defined with a sufficient precision by the incidence time of the XUV pulse. The final kinetic energy of an electron, which is measured by the PEEM, is found from the energy conservation,

$$E_{XUV}(\mathbf{r}, t_{XUV}) = \hbar\omega_{XUV} - W_f + e\varphi(\mathbf{r}, t_{XUV}), \tag{16}$$

where e is the electron charge, and $\mathbf{r}$ the emission point. In a sharp contrast to attosecond streaking in the gas phase [39], this energy does not depend on the initial momentum of the photoelectron or its subsequent flight trajectory.

Let us make estimates for the currently available XUV pulse parameters [40]: pulse duration $\tau_p = 170$ as and photon energy $\hbar\omega_{XUV} = 91$ eV. In such a case, assuming the workfunction $W_f = 5$ eV, we obtain the escape velocity $v_e = 5 \times 10^8$ cm s^{-1} and the escape time for the localization distance $b = 1$ nm as $\tau_e = 180$ as. Considering a near-infrared (NIR) driving pulse with a characteristic period $T \sim 3$ fs, we see that the instantaneous regime condition (15) is well satisfied for the optical field localization length that is up to several nanometres. Temporal resolution τ_r of the attosecond plasmonic field microscope is determined by both flight time τ_e through the region of nanolocalized optical fields and duration τ_p of the XUV pulse itself, $\tau_r \sim \tau_e + \tau_p$. For a NIR driving field and $b \lesssim 3$ nm, this resolution is sufficient, $\tau_r \ll T$. For visible excitation and plasmonic frequencies, sufficient temporal resolution can be achieved in the future with attosecond pulses delivered with photon energy $\hbar\omega_{XUV}$ of several hundred eV to a keV and duration below 100 as.

3.3. Fields as visualized by attosecond nanoplasmonic field microscope

Concentrating on this most important case of the instantaneous acceleration described by equations (15) and (16), we start with a model of a silver [41] random planar composite (whose geometry will be described below in the next paragraph). We apply an s-polarized (along the z-direction), waveform-controlled [30], 5.5 fs optical pulse $\mathbf{E}_0(t)$ shown in figure 1(a). We have computed local electric optical potential $\varphi(\mathbf{r}, t)$ and field $\mathbf{E}(\mathbf{r}, t)$ using the quasistatic spectral-expansion Green's function method [3, 15, 16], as given by equations (9) and (11). The excitation intensity is kept at a moderate level of $I = 10$ GW cm^{-2} to assure non-damaging conditions of the excitation. The carrier frequency of the optical (NIR) pulse is chosen to be 1.55 eV (corresponding to 800 nm vacuum wavelength). The temporal kinetics of the local field at a site where it reaches its global maximum is displayed in figure 1(b). It shows the initial period of the driven oscillations for $t < 20$ fs, where the response closely, albeit with a delay, reproduces the 5 fs excitation pulse, which reflects the sufficient bandwidth of this plasmonic system. At longer times, after the end of the excitation pulse, the free-induction evolution shows the interference beatings of several plasmonic eigenmodes. The maximum enhancement in this hot spot is $Q \approx 30$.

The random planar composite is generated as a collection of uncorrelated silver cubes (monomers) positioned on a plane in vacuum, which is illustrated in figure 2(a) for a monomer

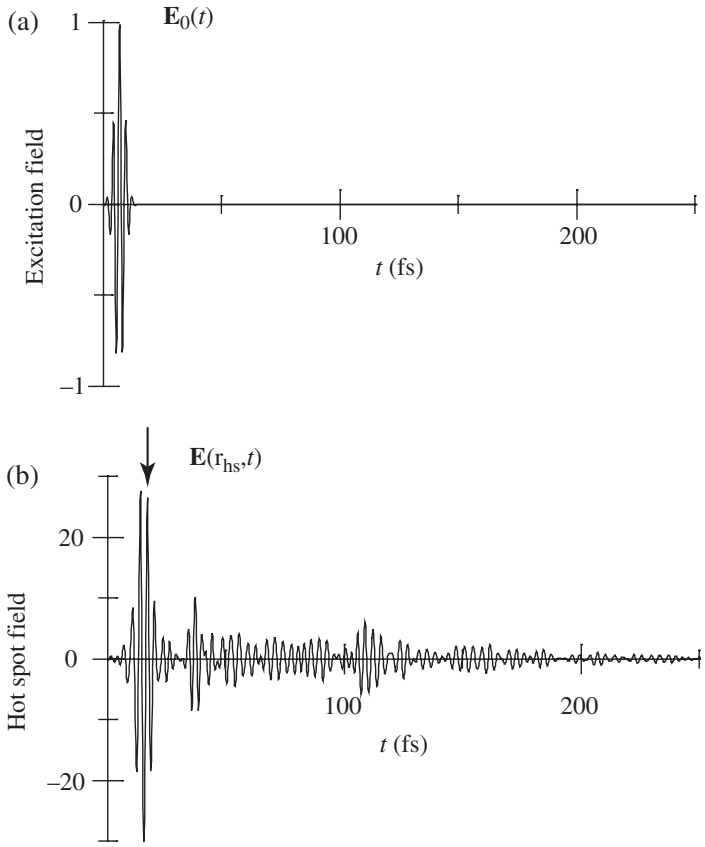

Figure 1. Excitation field and kinetics of the local field at a hot spot. (a) Excitation field $\mathbf{E}_0(t)$ as a function of time t. (b) Local field $\mathbf{E}(\mathbf{r}_{hs}, t)$ at the position $\mathbf{r}_{hs}$ of the maximum ('hottest spot') in figure 2(b) as a function of time t. The field magnitude is shown relative to the amplitude of the excitation pulse, which is set to 1. The vertical arrow denotes the oscillation period within which an XUV pulse is applied to probe the local field.

size of 4 nm. As characteristic of plasmonic nanosystems, there are 'hot spots' of the local fields induced by the optical excitation. The local field dynamics is shown in figure 1(b) for the 'hottest spot' where the local field reaches its global maximum in space and time. We assume that an XUV-attosecond pulse is incident at this system delayed with respect to the waveform-controlled [30] driving field in such a way that it probes the system close to the instance of the local field maximum (indicated by an arrow in figure 1(b)). According to equation (16), we compute the energy shift of an electron emitted by such an XUV pulse, which is due to the acceleration in the local plasmonic fields, as $\Delta E_{XUV}(\mathbf{r}, t_{XUV}) = e\varphi(\mathbf{r}, t_{XUV})$. We assume that these photoelectrons are spatially resolved by a PEEM and show in figures 2(b)–(f) a series of the electron energy distributions with an interval of $\Delta t_{XUV} \approx 400$ as during a half-period of the driving field. The distributions are shown as three-dimensional (3D) maps in (b)–(f). Even for the moderate excitation intensities used, the energy shift $|\Delta E_{XUV}|$ in hot spots of the plasmonic potential is rather large ($\sim$10 eV) and, consequently, relatively easily measurable. There is a pronounced nanometre–attosecond kinetics of the electron energy observed in these distributions with sharp hot spots indicative of those of the local fields. These hot spots are

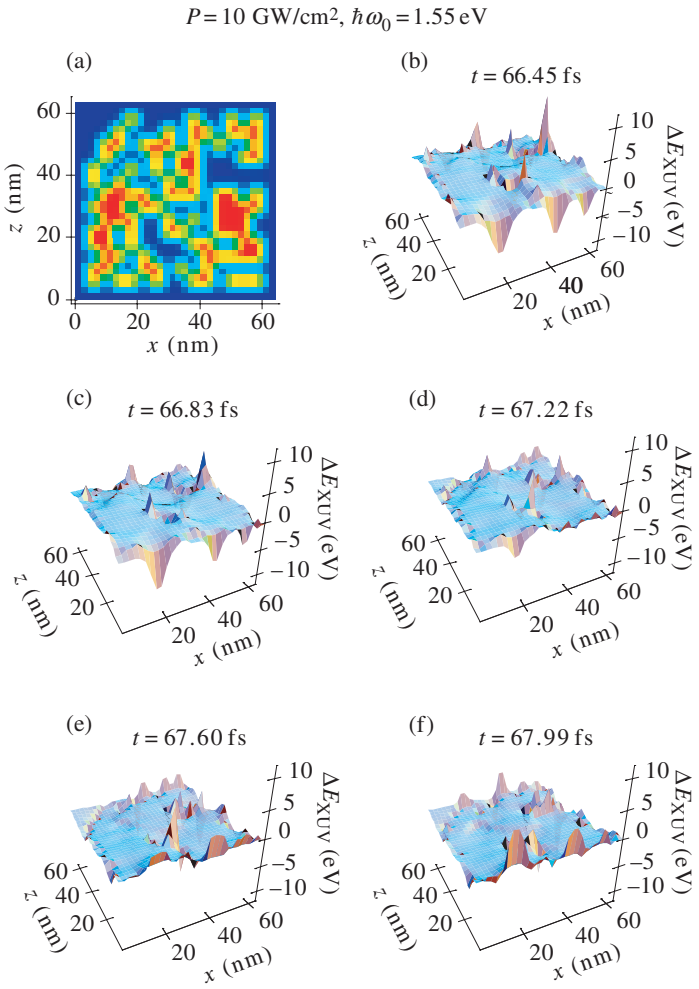

Figure 2. Topography of nanosystem and spatio-temporal kinetics of the local field potential as detected by an attosecond plasmonic field microscope. Intensity of the excitation optical pulse $P = 10\,\mathrm{GW\,cm^{-2}}$, and photon energy $\hbar\omega = 1.55\,\mathrm{eV}$. (a) Topography of the nanosystem: random planar composite consisting of $4 \times 4 \times 4\,\mathrm{nm}^3$ silver cubes arranged on a plane with fill factor 0.5. This composite is smoothed within 2 nm to improve numerical precision. (b)–(f) Distributions of energy shift ΔE_{XUV} of electrons emitted by an XUV pulse in the plane of this nanostructure shown as 3D maps for different moments t_{XUV} (as indicated in the panels) of the XUV pulse incidence within the half-cycle of local field oscillations.

concentrated around the edges and voids of the metal nanostructure as is a general trend in nanoplasmonics.

3.4. Discussion of attosecond nanoplasmonic field microscope

There are some interesting features of this proposed attosecond nanoplasmonic field microscope worth discussing. A remarkable property of this microscope is that it is, for any practical

purpose, non-invasive (non-perturbing). The attosecond XUV pulse is relatively very weak: the stream of such pulses in the microscope causes very weak ionization: the theory shows that they emit $\sim 10^3$ electrons per second only [4]. In contrast, the optical (infrared) field that excites the system can, in principle, be strong and cause significant nonlinear effects and ionization. However, these effects cannot be considered as perturbation, because they are present in the system anyway and are the subject of the study and, for a functional system, a part of its functioning.

The second point is that there are no wires or any other objects external to the system brought close to it to study its functioning such as, for instance, the tips of near-field microscopes [1], or the so-called superlenses or hyperlenses [14, 42], or metal wire arrays [43, 44]. Such metal objects in the nano-vicinity of the system would have been perturbing.

The third point is that the attosecond nanoplasmonic field microscope is an example of a device exploiting nonlinear interaction of electromagnetic pulses: one of them is the excitation optical (near-infrared) pulse, and the second is the attosecond pulse. On the other hand, it is an example of coherent control because spatial and energy distributions of the photoelectrons depend on the phase of the excitation optical radiation at the instance of the probing attosecond pulse. It is precisely the nonlinear phenomenon of this effect that makes possible the observation of the ultrafast fields by the PEEM, which is by itself a device without temporal resolution—cf [16].

4. Ultrafast coherent control by time reversal

4.1. Introduction to problem

The coherent control of the quantum state of atoms and molecules is based on the directed interference of the different quantum pathways of the optical excitation [45]–[51], which is carried out by properly defining the phases of the corresponding excitation waves. This coherent control can also be imposed by an appropriate phase modulation of the excitation ultrashort (femtosecond) pulse [48], [52]–[54]. Shaping the polarization of the excitation femtosecond pulse has proven to be a useful tool in controlling quantum systems [17].

It was predicted to be possible to coherently control the ultrafast spatial distribution of the optical excitation energy in nanostructures by pulse shaping (phase modulation) of an ultrashort excitation pulse [15, 16]. Such a control has been observed in the two-photon electron emission from silver nanostructured surfaces [19, 21]. Polarization-shaped pulses have been found to be an efficient tool in controlling the femtosecond dynamics of symmetric metal nanosystems [20, 55]. The coherent control of the electron emission by the phase-controlled XUV attosecond pulses superimposed on optical radiation recently has been proposed as the basis of an attosecond nanoplasmonic field microscope [4], which has been discussed above in section 3.

A major problem in the coherent control of the spatio–temporal (nanometre–femtosecond) dynamics of a nanosystem is the determination of a femtosecond optical waveform, which is phase-, amplitude-, and polarization-modulated, in the *far field* that would drive a nanosystem along such a pathway that at a desired time (with femtosecond precision) the optical energy will concentrate at a required site (with nanometre resolution). A theoretical, computational solution of this problem can be carried out, in principle, using genetic learning algorithms [48]. However, this procedure is cumbersome, and the obtained waveforms are often complicated and

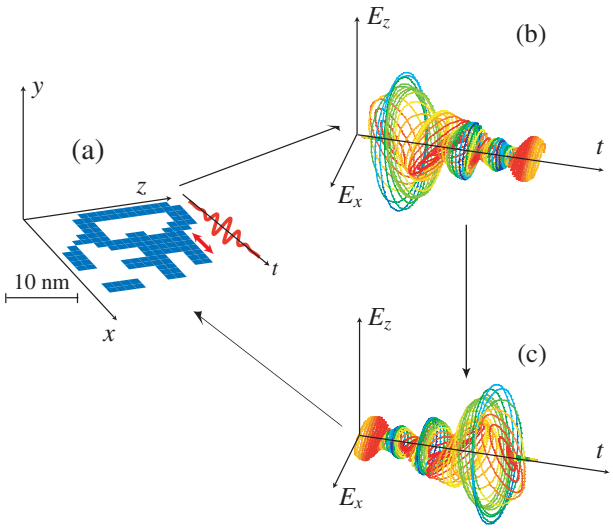

Figure 3. (a) Geometry of nanosystem, initial excitation dipole and its oscillation waveform. The nanosystem as a thin nanostructured silver film is depicted in blue. A position of the oscillating dipole that initially excites the system is indicated by a double red arrow, and its oscillation in time is shown by a bold red waveform. (b) Field in the far-field zone that is generated by the system following the excitation by the local oscillating dipole: vector $\{E_x(t), E_z(t)\}$ is shown as a function of the observation time t. The color corresponds to the instantaneous ellipticity as explained in the text in connection with (c), the same as in (b) but for a time-reversed pulse in the far zone that is used as an excitation pulse to drive the optical energy nanolocalization at the position of the initial dipole.

difficult to interpret (cf [21]). Our solution of this major problem is based on an idea of time-reversal that has originally been proposed and used to control the focusing of acoustic waves and microwave radiation [56]–[58]. These studies required use of a reverberating chamber to cause multiple interactions of the waves with the system needed to transfer the information to the far field. The electromagnetic subwavelength focusing also required a subwavelength-scale metal structure (a metal wire brush) to be positioned in the vicinity of the target system as a focusing antenna. In contrast, in nanoplasmonics there is no need for the reverberating chamber or the metal brush antenna, because the plasmonic nanosystem plays the roles of both of them. It confines the plasmonic modes for long times relative to their oscillation periods and also nano-localizes these modes.

4.2. Principles of time-reversal solution for coherent control

The idea of our time-reversal solution [22] of nanoscale coherent control can be described using the schematic of figure 3. A nanosystem is excited by an external ultrafast (femtosecond) nanosource of radiation at its surface. As such we chose an oscillating dipole indicated by a double red arrow in figure 3(a). This dipole generates a local optical electric field shown by a bold red waveform. This field excites SP oscillations of the system in its vicinity; in turn these oscillations excite other, more distant regions, and so forth until the excitation spreads out over the entire system. The relatively long relaxation time of these SP modes leads to the

long 'reverberations' of the plasmonic fields and the corresponding far-zone optical electric field. The latter is shown in figure 3(b) where one can see that a complicated vector waveform is predicted. This waveform is time reversed, as shown in figure 3(c), and sent back to the system as an excitation plane wave from the *far* zone. If the entire field, in the whole space including the near-field (evanescent) zone, were time reversed *and* the system were completely time-reversible, which would imply the absence of any dielectric losses, then the system would have been compelled by this field exactly to back-trace its own evolution in time. This would have lead to the concentration of the local optical energy exactly at the position of the initial dipole at a time corresponding to the end of the excitation pulse.

Indeed, the system is somewhat lossy, which means that it is not exactly time reversible. Nevertheless, these losses are small, and one may expect that they will not principally change the behavior of the system. Another problem appears to be more significant: the evanescent fields contain the main information on the nano-distribution of the local fields in the system, and they cannot be time reversed from the far zone because they are exponentially small, practically lost there. However, our idea is that the nanostructured metal system itself plays the role of the metal brush of [58] continuously coupling the evanescent fields to the far zone. Therefore the fields in the far zone actually contain, in their reverberations, most information about the evanescent fields that will be regenerated in the process of the time reversal. These two arguments, regarding the possibility to neglect the losses and the regeneration of the near-fields, of course, should and will be scrutinized and confirmed by our computations presented later in this paper.

4.3. System and computation procedure

We will illustrate our idea by considering a random plasmonic nanolayer whose geometry is shown in gray at the bottom of figure 4. In specific computations, as the plasmonic metal, we consider silver whose dielectric permittivity ε_{m} we adopt from bulk data [41]. This system has been generated by randomly positioning $2 \times 2 \times 2\,\mathrm{nm}^3$ metal cubes on a plane, which for certainty we will consider as the xz-coordinate plane. The random system shown at the bottom of figure 4 has filling factor of 0.5.

The interaction of a nanosystem with electromagnetic pulses is described in Green's function approach using quasistatic approximation [15, 16, 24]; some necessary details of this approach are given above in section 2.2. It is known that the optical excitation energy in random plasmonic nanostructures localizes in 'hot spots' whose size is on the nanoscale and is determined by the minimum scale of the system inhomogeneities [3, 59, 60]. Initially, to find positions of these hot spots in our system, we apply an ultrashort NIR pulse whose spectral width was very large, covering a band from 1.1 to 1.7 eV. The pulse polarization is along the z-axis (the incidence direction is normal to the plane of the nanostructure, i.e. along the y-axis). The resulting optical electric field $\mathbf{E}$ is expressed in terms of the external electric field of the excitation optical wave $\mathbf{E}_0$ and retarded dyadic Green's function $\mathbf{G}^{\mathrm{r}}$ by equation (11).

The hot spots are always localized at the surface of the metal, predominantly at the periphery of the system. Their intensities found as the result of these computations are depicted by colors at the bottom of figure 4. The highest local intensity is indicated by red, and the lowest by blue in the region surrounding the metal. We have randomly selected two of these hot spots for our computations as denoted by letters A and B in the figure.

To generate the field in the far zone, we take a point dipole and position it at a surface of the metal at point $\mathbf{r}_0$ at such a hot spot, as described in the discussion of figure 3 above. The

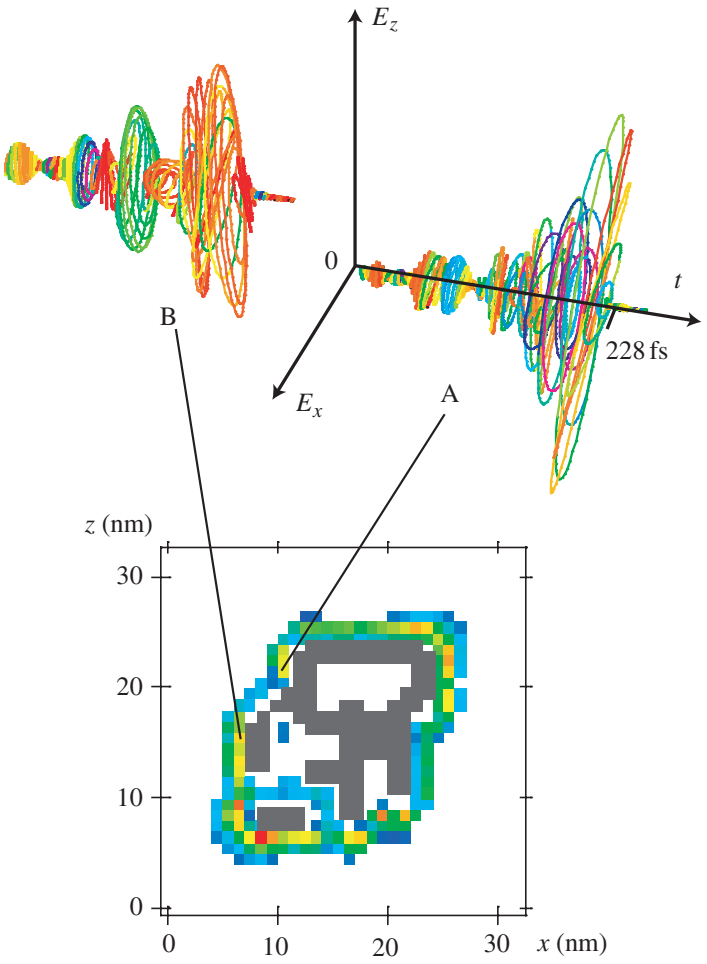

Figure 4. Schematic of plasmonic-nanosystem geometry, local fields, and pulses generated in the far field. Insert: the geometry of a nanosystem is shown by dark gray, and the local fields in the region surrounding it are shown by colors. The highest local field intensity is depicted by red and the lowest intensity is indicated by blue (in the rainbow sequence of colors). Panels A and B: the excitation waveforms in the far fields obtained as described in the text by positioning the initial excitation dipole at the metal surface at the locations indicated by the corresponding lines. Coordinate vectors ρ of points A and B in the xz-plane are (in nm): $\rho_{\mathrm{A}} = (11, 22)$ and $\rho_{\mathrm{B}} = (7, 16)$. The instantaneous degree of linear polarization ε is calculated as the eccentricity of an instantaneous ellipse found from a fit to a curve formed by vector $\{E_x(t), E_y(t)\}$ during an instantaneous optical period. The pure circular polarization corresponds to $\varepsilon = 0$ and is denoted by blue-violet color; the pure linear polarization is for $\varepsilon = 1$ indicated by red.

near-zone field $\mathbf{E}^{\mathrm{L}}(\mathbf{r}, t)$ generated in response to this point dipole is found from the Green's function relation as equation (14). Knowing this local electric field, we calculate the total radiating optical dipole moment of the nanosystem in the frequency domain as

$$\mathbf{D}(\omega) = \frac{1}{4\pi} \int \mathrm{d}^3 r \, [\varepsilon_{\mathrm{m}}(\omega) - \varepsilon_{\mathrm{d}}] \, \Theta(\mathbf{r}) \mathbf{E}^{\mathrm{L}}(\mathbf{r}, \omega). \tag{17}$$

To recall our convention, here and everywhere the frequency- and time-domain quantities, as indicated by their arguments ω and t, are Fourier transforms of each other. The field in the far zone produced by this radiating dipole is given by a standard electrodynamic formula (see, e.g. equation (67) in [61]). The time-reversed field is generated by the time-reversed dipole $\mathbf{D}^{\mathrm{T}}(t)$ that is complex-conjugated in the frequency domain, $\mathbf{D}^{\mathrm{T}}(\omega) = \mathbf{D}(\omega)^*$.

The dependence on time of the initial excitation dipole, $\mathbf{d}(\mathbf{r}_0, t)$ was an ultrashort Gaussian-shaped pulse of 12 fs duration with the carrier frequency $\hbar\omega_0 = 1.2$ eV. Following the procedure described above, the fields shown in figures 3 and 4 have been calculated for the radiation propagating in the y-direction (normal to the plane of the nanostructure). These fields simply copy the retarded time evolution of the emitting dipole.

In the final stage of our calculations, the time-reversed excitation pulse is sent back to the system as a plane wave propagating along the y-direction (normal to the nanosystem plane). To calculate the resulting local fields, we again use Green's function equation (11), where the shaped excitation pulse substitutes for field $\mathbf{E}_0$.

4.4. Excitation pulses

The electric field of the excitation wave was a modulated waveform (including amplitude, phase and polarization modulation) that has been computed as described above in the previous subsection. The optical excitation energy can only be concentrated at sites where SP eigenmodes localize. For the present system, these are the hot spots shown by color at the bottom of figure 4. The corresponding calculated excitation waveforms are displayed in panels as vector plots shown as functions of time $\{E_x(t), E_z(t)\}$. The computation results are shown for two hot spots labeled as A and B, which are considered as an example.

There are several important features of these waveforms deserving our attention and discussion. Firstly, these waveforms are rather long in duration: much longer than the excitation-dipole 12-fs pulses. This confirms our understanding that the initial dipole field excites local SP fields that, in a cascade manner, excite a sequence of the system SPs, which ring down for a relatively long time (over 200 fs, as shown in the figure). This long ring-down process is exactly what is required for the nanostructure to transfer to the far-field zone the information on the near-zone local (evanescent) fields as is suggested by our idea presented above in the introduction. The obtained fields are by shape very similar to the controlling pulses for the microwave radiation [58]. However, a principal difference is that in the microwave case the long ringing-down is due to the external reverberation chamber, while for the nanoplasmonic systems it is due to the intrinsic evolution of the highly resonant SP eigenmodes that possess high Q-factors (setting a reverberation chamber around a nanosystem would have been, indeed, unrealistic).

Secondly, one can see that the pulses in figure 4 have very nontrivial polarization properties ranging from pure linear polarization (indicated by red as explained in the caption to figure 4) to circular polarization indicated by blue, including all intermediate degrees of circularity. The temporal-polarization structure of pulses A and B in figure 4 is very complicated, somewhat reminiscent of that of [20], which was obtained by a genetic adaptive algorithm. However, in our case these pulses are obtained in a straightforward manner, by applying the well-known, deterministic Green's function of the system, which is a highly efficient and fast method.

The third, and most important, feature of the waveforms in figure 4 is that they are highly site-specific: pulses generated by the initial dipole in different positions are completely different.

This is a very strong indication that they do transfer to the far far-field zone the information about the complicated spatio-temporal structure of the local, near-zone fields. This creates a pre-requisite for studying a possibility to use these pulses for the coherently-controlled nano-targeting.

4.5. Coherent control of spatio-temporal energy distribution on the nanoscale by time reversal

Now, we turn to the crucial test of the nanofocusing induced by the excitation pulses discussed above in conjunction with figure 4. Because of the finite time window ($T = 228$ fs) used for the time reversal, all these excitation pulses end and should cause the concentration of the optical energy (at the corresponding sites) at the same time, $t = T = 228$ fs (counted from the moment the excitation pulse starts impinging on the system). After this concentration instant, the nanofocused fields can, in principle, disappear (dephase) during a very short period on the order of the initial dipole pulse length, i.e. $\sim$10 fs. Thus this nanofocusing is a dynamic, transient phenomenon.

Note that averaging (or, integration) of the local-field intensity $I(\mathbf{r}, t) = |\mathbf{E}(\mathbf{r}, t)|^2$ over time t would lead to the loss of the effects of the phase modulation. This is due to a mathematical equality $\int_{-\infty}^{\infty} I(\mathbf{r}, t)\,\mathrm{d}t = \int_{-\infty}^{\infty} |\mathbf{E}(\mathbf{r}, \omega)|^2\,\mathrm{d}\omega/(2\pi)$, where the phase of the field is certainly eliminated from the expression in the right-hand side. Thus the averaged intensity of the local fields is determined only by the local power spectrum of the excitation $|\mathbf{E}(\mathbf{r}, \omega)|^2$ and, consequently, is not coherently controllable. Very importantly, such a cancellation is not valid for nonlinear phenomena. In particular, two-photon processes such as two-photon fluorescence or two-photon electron emission that can be considered as proportional to the squared intensity $I^2(\mathbf{r}, t) = |\mathbf{E}(\mathbf{r}, t)|^4$ are coherently controllable even after time averaging (integration), as we have argued earlier [16, 62]. Note the distributions measured in nonlinear optical experiments with the detection by the photoemission electron microscope (PEEM) [19]–[21], [63] and in the fluorescence upconversion experiments [11] can be modeled as such nonlinear processes that yield distributions $\langle I^n(\mathbf{r})\rangle = \int_{-\infty}^{\infty} I^n(\mathbf{r}, t)\mathrm{d}t/T$, where $n \geqslant 2$. Inspired by this, we will also consider below the coherent control of the two-photon process averaged intensity $\langle I^2(\mathbf{r})\rangle$.

To establish the controlled nanofocusing and elucidate the role of the polarization pulse shaping, we start by comparing two pulses A and B. As we see from figure 4, these pulses are very different, including their amplitude, phase and polarization. Note that both the pulses contain significant components of circularity indicated by green–blue colors, which suggests the importance of the polarization modulation. The results of computations using these two pulses are shown in figure 5. Note that the excitation pulses used in the computations have not been specially normalized. Thus only the distribution of the intensities is meaningful but not their absolute magnitude that depends on the arbitrary excitation pulse power.

We first investigate precisely how one can address the optical excitation of a given nanosite at a plasmonic nanostructure using the excitation pulses as found from the time-reversal method. The results for the local field intensity distributions for the present nanostructure, targeting sites A and B, are shown in figures 5(a) and (b). In these panels, for each excitation pulse, the spatial distribution of the local field intensity is displayed for the moment of time when this local intensity acquires its global (highest) maximum. The most important conclusion that one can draw from comparing these panels is that for each pulse this global maximum corresponds to the maximum concentration of the optical energy at the corresponding targeted nanosite A or B. This obtained spatial resolution is as good as 4 nm, which is determined by the spatial size

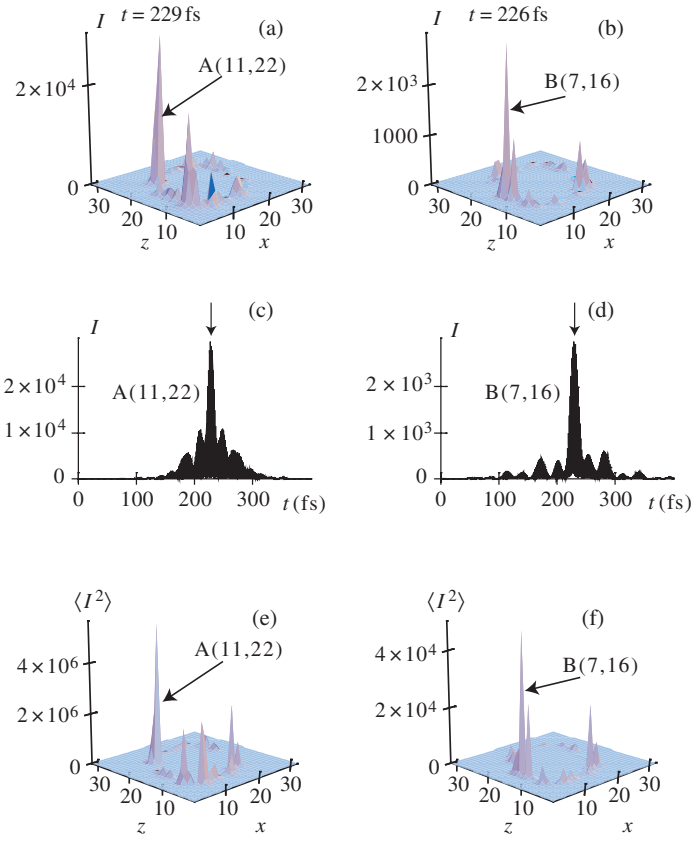

Figure 5. Calculation results demonstrating time-reversal coherent control on the nanoscale. Panels (a) and (b) display distributions of the local field intensity at the surface of the metal nanostructure for the moments of time t indicated when the intensities at the targeted sites reaches their maxima. The fields are excited by the pulses obtained for targeted sites A and B using the corresponding pulses indicated in figure 4. Panels (c) and (d) show temporal dependence of the local field intensity $I(\mathbf{r}, t) = |\mathbf{E}(\mathbf{r}, t)|^2$ computed for targeted points A and B, respectively. The arrows show the target time $T = 228$ fs. Panels (e) and (f) are similar to (a) and (b), correspondingly, but show the time-averaged square intensity $\langle I^2(\mathbf{r})\rangle$.

of inhomogeneities of the underlying plasmonic metal nanosystem. It is very important that this localization occurs not only at the desired nanometre-scale location but also very close to the targeted time that in our case is $t = 228$ fs. Thus the full shaping of femtosecond pulses by time reversal is an efficient method of controlling the spatio-temporal localization of energy at the femtosecond–nanometre scale.

Let us turn to the temporal dynamics of the intensity of the nanoscale local fields at the targeted sites A and B, which is shown in figures 5(c) and (d). As we can see, in each of these panels there is a sharp spike of the local fields very close to the target time of 228 fs. The duration of this spike is close to that of the initial dipole pulse, i.e. 12 fs. This shows a trend to the reproduction of the initial excitation state due to the evolution of the time-reversed SP packet induced by the shaped pulses. There is also a pedestal that shows that this reproduction is not precise, which is expected due to the fact that the time reversal is incomplete: only the

far-zone field propagating in one direction (along the y-axis) is reversed. Nevertheless, as the discussion in the previous paragraph shows, this initial excitation-state reproduction is sufficient to guarantee that the targeted site develops the global maximum (in time and space) of the local field intensity. Interestingly enough, the trend to reproduce the initial excitation state is also witnessed by almost symmetric (with respect to the maximum points $t \approx 228$ fs) shapes of the waveforms, which occur in spite of the very asymmetric shapes of the excitation waveforms (cf figure 4).

Apart from the ultrafast dynamics of the nanolocalized optical fields discussed above in conjunction with figure 5(a)–(d), there is a great interest in the time-integrated or averaged distributions, in particular, the mean squared intensity $\langle I^2(\mathbf{r})\rangle$. This quantity defines the nanoscale spatial distribution of the incoherent two-photon processes. In some approximations, the spatial distribution of the two-photon electron emission recorded by PEEM [19]–[21], [63] is determined by $\langle I^2(\mathbf{r})\rangle$. In figure 5(e) and (f), we test such a concentration for the A and B sites. As clearly follows from this figure, in both cases, there are leading peaks at the targeted sites. Thus, the two-photon excitation, even after the time averaging, can be concentrated at desired sites using coherent control by the time-reversed shaped pulses.

4.6. Discussion of ultrafast coherent control by time reversal

The spatio-temporal control of the optical excitation of a nanosystem on a nanometre–femtosecond scale is one of the most important and fundamental problems of nanoplasmonics and nanotechnology. In the conventional microelectronics, this problem is solved using metal (currently, copper) wire interconnects. However, for optical frequencies and nanometre spatial dimensions, this approach cannot work because of the excitation delocalization due to the strong interaction at the nanoscale distances. We have proposed a principally different approach to this formidable problem that is based on the idea of coherent control that is a directed interference between a system's eigenmodes [15]. In this approach, one does not attempt a localized excitation of a plasmonic nanosystem: generally, such an excitation will delocalize over the entire system during femtosecond time intervals. On the contrary, one excites a wide-band packet of SP excitations in the entire system. The phases, amplitudes, and polarizations of these modes are forced by the excitation pulse in such a way that at the required moment of time and at the targeted nanosite, these modes' oscillations add in phase while at the other sites and different moments of time they interfere destructively.

This idea allows a targeted ultrafast (femtosecond-scale) and localized (nanometre-scale) excitation but is completely dependent on the possibility of finding the corresponding controlling pulse that is, in a general case, fully modulated by amplitude, phase and polarization. Finding such a pulse to target a specific location in a nanosystem is a formidable problem that, in principle, could be solved by using adaptive algorithms [48, 49]. However, the solutions obtained by this method are computationally taxing, can be very complicated even for simple systems [20] and are difficult to interpret.

In this section, we have discussed a principally different approach [22] based on the idea of time reversal. Nanoplasmonic systems of noble metals in the optical range of frequencies have high resonant quality (low losses) and therefore, in principle, are almost time reversible. However, a significant problem is that the evanescent (near-zone) fields are vanishingly (exponentially) small in the far zone and therefore cannot be reversed. An original idea to overcome this difficulty in acoustics and microwave electromagnetics was to put a system into

a reverberating box to increase the time of the wave interaction with the system to transfer the information from the near- to far-field zone [56]–[58]. Putting a nanosystem into such a box is, of course, impractical.

Our present idea is that a plasmonic nanosystem itself, due to its high resonant quality, traps and sustains the optical oscillations for a relatively long time (∼100 fs). The oscillating optical fields continuously interact with the plasmonic nanostructure, transferring the information from the evanescent (near-zone) fields to radiative (far-zone) fields where it is encoded into the field temporal dynamics. Direct evidence of such a transfer is illustrated in figure 4, where the waveforms emitted by the locally excited nanosystem are long, reverberating, and *highly specific* for the position of the initial excitation.

This local excitation has been carried out in our theory by placing a dipole close to the targeted nanosite and giving this pulse a short (12 fs) Gaussian-shaped pulse of oscillations at a near-infrared frequency that is within the resonant spectrum of the nanostructure. The orientation of this dipole was chosen either along the x- or z-direction, with no significant differences found between these two orientations; the x-orientation was chosen to present the results.

Such an approach can, in principle, be implemented not only theoretically but also experimentally by positioning a fluorescent emitter (for example, a semiconductor nanocrystal quantum dot) at the desired site of the nanosystem and exciting it externally with an optical pulse in the ultraviolet that does not by itself cause a resonant response of the nanosystem. Such quantum dots are photochemically stable emitters, and accumulating statistics over many pulses one can find the field of the pulse in the far zone. The required time-reversal can then be effected using the standard pulse-shaping techniques.

The proposed method of time-reversal coherent control is efficient and noninvasive: this control is carried out from the far zone using the nanoplasmonic system itself as an optical nanoantenna without any additional metal parts. Another potential approach of coupling nanosystems to the far-zone fields could consist of the use of the so-called magnifying superlenses (‘perfect lenses’) [64], hyperlenses [14], or adiabatic concentrators [10] including those based on metal-wire arrays [43, 44]. In all these cases, a massive amount of metal would be brought into the vicinity of the plasmonic nanosystem, which will cause correspondingly massive perturbations of the spectrum and SP eigenmodes, losses, etc. With respect to all these methods, which together can be called nano-waveguide approaches, our proposed time-reversal coherent control has the great potential advantages of being wireless, noninvasive, fast, and having a high spatial resolution on the nanoscale, unattainable by other approaches.

Now let us discuss potential applications of the targeted excitation of a nanosystem with shaped optical pulses, which may be many. One of the first and, potentially most important, applications is that to ultrafast (with frequencies from terahertz to optical) computations on the nanoscale. As follows from the results presented above in section 4.5, it is possible to supply optical energy (which can be transformed on-site into electrical energy using optical rectification) and controlling pulses to plasmonic nanocircuits or electronic nanochips with optical plasmonic antennas. Another class of applications is in time-resolved local spectroscopy with nanoscale resolution, or directed photochemistry on the nanoscale. Related are applications to optical recording and retrieval of information with nanoscale density of bits. Yet another application may be the creation of nanoscale sources of ultrashort electron-beam pulses, which could find their own application in the future. Many other potential applications may be possible that is hard even to foresee at this time.

Acknowledgments

This work was supported by grants from the Chemical Sciences, Biosciences and Geosciences Division of the Office of Basic Energy Sciences, Office of Science, US Department of Energy, a grant CHE-0507147 from NSF, and a grant from the US–Israel BSF.

References

[1] Novotny L and Hecht B 2006 *Principles of Nano-Optics* (Cambridge: Cambridge University Press)
[2] Kawata S (ed) 2001 *Topics in Applied Physics* vol 81 (Berlin: Springer)
[3] Stockman M I, Faleev S V and Bergman D J 2001 *Phys. Rev. Lett.* **87** 167401
[4] Stockman M I, Kling M F, Kleineberg U and Krausz F 2007 *Nat. Photonics* **1** 539
[5] Klar T, Perner M, Grosse S, von Plessen G, Spirkl W and Feldman J 1998 *Phys. Rev. Lett.* **80** 4249
[6] Lehmann J, Merschdorf M, Pfeiffer W, Thon A, Voll S and Gerber G 2000 *Phys. Rev. Lett.* **85** 2921
[7] Bosbach J, Hendrich C, Stietz F, Vartanyan T and Trager F 2002 *Phys. Rev. Lett.* **89** 257404
[8] Hendrich C, Bosbach J, Stietz F, Hubenthal F, Vartanyan T and Trager F 2003 *Appl. Phys.* B **76** 869
[9] Zentgraf T, Christ A, Kuhl J and Giessen H 2004 *Phys. Rev. Lett.* **93** 243901
[10] Stockman M I 2004 *Phys. Rev. Lett.* **93** 137404
[11] Verhagen E, Kuipers L and Polman A 2007 *Nano Lett.* **7** 334
[12] Gramotnev D K and Vernon K C 2007 *Appl. Phys.* B **86** 7
[13] Ropers C, Neacsu C C, Elsaesser T, Albrecht M, Raschke M B and Lienau C 2007 *Nano Lett.* **7** 2784
[14] Liu Z, Lee H, Xiong Y, Sun C and Zhang X 2007 *Science* **315** 1686
[15] Stockman M I, Faleev S V and Bergman D J 2002 *Phys. Rev. Lett.* **88** 067402
[16] Stockman M I, Bergman D J and Kobayashi T 2004 *Phys. Rev.* B **69** 054202
[17] Brixner T, Krampert G, Pfeifer T, Selle R, Gerber G, Wollenhaupt M, Graefe O, Horn C, Liese D and Baumert T 2004 *Phys. Rev. Lett.* **92** 208301
[18] Sukharev M and Seideman T 2006 *Nano Lett.* **6** 715
[19] Kubo A, Onda K, Petek H, Sun Z, Jung Y S and Kim H K 2005 *Nano Lett.* **5** 1123
[20] Aeschlimann M, Bauer M, Bayer D, Brixner T, Abajo F J G d, Pfeiffer W, Rohmer M, Spindler C and Steeb F 2007 *Nature* **446** 301
[21] Bauer M, Wiemann C, Lange J, Bayer D, Rohmer M and Aeschlimann M 2007 *Appl. Phys.* A **88** 473
[22] Li X and Stockman M I 2007 *Preprint* 0705.0553
[23] Bergman D J and Stockman M I 2003 *Phys. Rev. Lett.* **90** 027402
[24] Stockman M I 2006 *Surface Enhanced Raman Scattering—Physics and Applications* ed K Kneipp, M Moskovits and H Kneipp (Berlin: Springer) pp 47–66
[25] Bergman D J and Stroud D 1992 *Solid State Physics* vol 46 ed H Ehrenreich and D Turnbull (New York: Academic) pp 148–270
[26] Paul P M, Toma E S, Breger P, Mullot G, Auge F, Balcou P, Muller H G and Agostini P 2001 *Science* **292** 1689
[27] Hentschel M, Kienberger R, Spielmann C, Reider G A, Milosevic N, Brabec T, Corkum P, Heinzmann U, Drescher M and Krausz F 2001 *Nature* **414** 509
[28] Niikura H, Legare F, Hasbani R, Bandrauk A D, YIvanov M, Villeneuve D M and Corkum P B 2002 *Nature* **417** 917
[29] Drescher M, Hentschel M, Kienberger R, Uiberacker M, Yakovlev V, Scrinizi A, Westerwalbesloh T, Kleineberg U, Heinzmann U and Krausz F 2002 *Nature* **419** 803
[30] Baltuska A *et al* 2003 *Nature* **421** 611
[31] Niikura H, Legare F, Hasbani R, Ivanov M Y, Villeneuve D M and Corkum P B 2003 *Nature* **421** 826
[32] Kienberger R *et al* 2004 *Nature* **427** 817
[33] Sekikawa T, Kosuge A, Kanai T and Watanabe S 2004 *Nature* **432** 605

[34] Lopez-Martens R *et al* 2005 *Phys. Rev. Lett.* **94** 033001
[35] Baker S, Robinson J S, Haworth C A, Teng H, Smith R A, Chirila C C, Lein M, Tisch J W G and Marangos J P 2006 *Science* **312** 424
[36] Dudovich N, Smirnova O, Levesque J, Mairesse Y, Ivanov M Y, Villeneuve D M and Corkum P B 2006 *Nat. Phys.* **2** 781
[37] Sansone G *et al* 2006 *Science* **314** 443
[38] Kling M F *et al* 2006 *Science* **312** 246
[39] Corkum P B and Krausz F 2007 *Nat. Phys.* **3** 381
[40] Schultze M, Goulielmakis E, Uiberacker M, Hofstetter M, Kim J, Kim D, Krausz F and Kleineberg U 2007 *New J. Phys.* **9** 243
[41] Johnson P B and Christy R W 1972 *Phys. Rev.* B **6** 4370
[42] Smolyaninov I I, Hung Y-J and Davis C C 2007 *Science* **315** 1699
[43] Ono A, Kato J and Kawata S 2005 *Phys. Rev. Lett.* **95**
[44] Shvets G, Trendafilov S, Pendry J B and Sarychev A 2007 *Phys. Rev. Lett.* **99** 053903
[45] Kurizki G, Shapiro M and Brumer P 1989 *Phys. Rev.* B **39** 3435
[46] Weinacht T C, Ahn J and Bucksbaum P H 1999 *Nature* **397** 233
[47] Brumer P and Shapiro M 1992 *Annu. Rev. Phys. Chem.* **43** 257
[48] Rabitz H, de Vivie-Riedle R, Motzkus M and Kompa K 2000 *Science* **288** 824
[49] Geremia J M and Rabitz H 2002 *Phys. Rev. Lett.* **89** 263902
[50] Nguyen N A, Dey B K, Shapiro M and Brumer P 2004 *J. Phys. Chem.* A **108** 7878
[51] Shapiro M and Brumer P 2006 *Phys. Rep.* **425** 195
[52] Assion A, Baumert T, Bergt M, Brixner T, Kiefer B, Seyfried V, Strehle M and Gerber G 1998 *Science* **282** 919
[53] Bartels R, Backus S, Zeek E, Misoguti L, Vdovin G, Christov I P, Murnane M M and Kapteyn H C 2000 *Nature* **406** 164
[54] Dudovich N, Oron D and Silberberg Y 2002 *Nature* **418** 512
[55] Brixner T, Garcia de Abajo F J, Schneider J and Pfeiffer W 2005 *Phys. Rev. Lett.* **95** 093901
[56] Derode A, Tourin A, de Rosny J, Tanter M, Yon S and Fink M 2003 *Phys. Rev. Lett.* **90** 014301
[57] Lerosey G, de Rosny J, Tourin A, Derode A, Montaldo G and Fink M 2004 *Phys. Rev. Lett.* **92** 193904
[58] Lerosey G, de Rosny J, Tourin A and Fink M 2007 *Science* **315** 1120
[59] Stockman M I, Pandey L N, Muratov L S and George T F 1995 *Phys. Rev.* B **51** 185
[60] Stockman M I 1997 *Phys. Rev. Lett.* **79** 4562
[61] Landau L D and Lifshitz E M 1975 *The Classical Theory of Fields* (Oxford: Pergamon)
[62] Stockman M I and Hewageegana P 2005 *Nano Lett.* **5** 2325
[63] Kubo A, Pontius N and Petek H 2007 *Nano Lett.* **7** 470
[64] Pendry J B 2003 *Opt. Express* **11** 755